

RESEARCH ARTICLE

Techno-Economic Optimization of the NbTi DTT Feeders

DANIELE PLACIDO¹, GIANLUCA DE MARZI², LUIGI MUZZI², (Senior Member, IEEE),
AND LAURA SAVOLDI¹, (Member, IEEE)

¹Dipartimento Energia “Galileo Ferraris”, Politecnico di Torino, 10129 Turin, Italy

²FNS Department, Superconductivity Section, ENEA Frascati Research Center, 00044 Frascati, Italy

Corresponding author: Laura Savoldi (laura.savoldi@polito.it)

ABSTRACT The superconducting (SC) coils of the Divertor Tokamak Test (DTT) facility will be connected to the current leads by a set of SC feeders, currently designed as cable-in-conduit conductors wound using commercial NbTi strands to be cooled by Supercritical Helium at 4.5 K. The feeders are immersed in the magnetic field generated by the SC coil and plasma outside of magnet system, so that the maximum field on the most loaded feeder can reach 4 T at the full rated current (including the self-field effect). Here the performance of the feeder conductors is assessed during a plasma pulse, based on the DTT standard single-null operating scenario, for the most loaded feeder of the Central Solenoid and of the Toroidal and Poloidal Field coils, computing the minimum temperature margin to current sharing throughout the plasma scenario. Several alternative cabling configurations are analyzed, designed to withstand the nominal current at the peak field with a different number of SC and stabilizer strands. The minimum temperature margin is evaluated as a function of the material, manufacturing and operational costs of the different alternative feeder layouts. Based on such techno-economical characterization, the optimal (cheapest) design of the feeder cables is identified.

INDEX TERMS DTT facility, superconducting cables, cable-in-conduit conductors, current leads, temperature margin, techno-economic analysis.

I. INTRODUCTION

In the framework of the European Roadmap to Nuclear Fusion [1], the DTT (Divertor Tokamak Test) facility [2] is currently under construction at ENEA, Frascati. The machine is fully superconductive [3], similarly to the largest tokamaks in operation (e.g. KSTAR [4] and EAST [5]), commissioned (JT-60SA [6]) and under construction (ITER [7], SPARC [8]) worldwide. Like in the JT-60SA design, the current to the superconducting (SC) magnets arrives from the power supply at room temperature through the busbar to the current leads, contained in the Cold Terminal Boxes (CTB). The current leads transfer the transport current from their “hot” termination at room temperature to their “cold” termination at cryogenic temperature, electrically joined to the SC feeders. In turn the feeders, contained inside three cryolines that protrude out of the cryostat surrounding the tokamak in the

tokamak hall, transfer the transport current to the SC coil, see Fig. 1.

The current design of the feeders consists of cable-in-conduit conductors (CICC) [9] wound using commercial NbTi strands to be cooled by Supercritical Helium at 4.5 K [10]. The feeders are immersed in the magnetic field generated by the SC coils and plasma outside of magnet system, so that the maximum field on the most loaded feeder can reach 4 T at the full rated current (including the self-field effect). A first design of all feeders has been already performed in DC condition, checking that the temperature margin to current sharing ΔT_{CS} at the nominal current is $> 2\text{K}$ for all feeders [10]. This first design step was quite straightforward, since it was based on a well-established scaling for the strand critical current [11], considering the nominal operating temperature of 4.5 K. In DC condition, the temperature computed along the feeders turned out to be totally acceptable in view of the short length of the feeders and of a small effect of the radiative load from the thermal

The associate editor coordinating the review of this manuscript and approving it for publication was Vlad Diaconita¹.

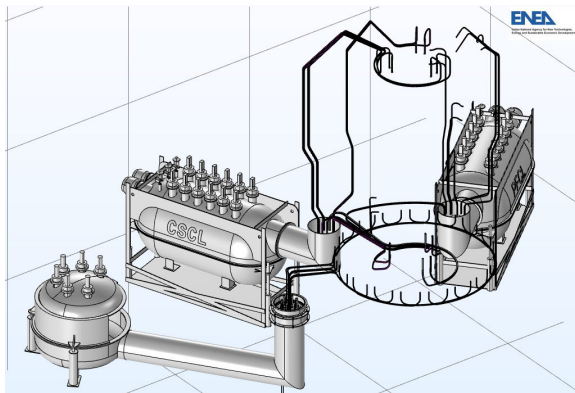


FIGURE 1. Layout of the SC feeders and cryolines for the DTT machine: CSCL: Central Solenoid Current Leads box; PFCL: Poloidal Field Current Leads box; and TFCL (bottom left) Toroidal Field Current Leads box.

shield, and Joule losses foreseen in the joint to the coil cables.

However, the design so far has not been checked yet in operative (transient) conditions during a plasma pulse, where on one hand, for the pulsed coils (Central Solenoid CS, and Poloidal Field PF coils), the current and induced magnetic field variation lead to significant heating in the cable due to AC losses, while, on the other hand, the feeders of the DC Toroidal Field (TF) coils - where AC losses are expected to be very small - are subject to nuclear heating [12]. Note that the conductor design in DC conditions could be not optimal for the AC conditions of the pulsed coils, in view of the strongly transient nature of the heat load deposited in the conductor.

The aim of this paper is to perform a techno-economical assessment of the DTT feeder conductors, considering also their transient performance. Based on the DTT standard operating scenario, here the performance of the feeder conductors in operation is assessed in terms of the minimum margin ΔT_{CS}^{min} throughout the standard single-null plasma scenario. In the margin assessment, the radiative load from the thermal shield inside the machine cryostat, as well as the Joule heating in the terminations is accounted for. Several possible alternative designs are considered for the most critical feeder for the CS, PF coils and TF coils. The related variation of the minimum ΔT_{CS}^{min} is investigated as a function of the cost related to the cable design (number of SC and stabilizer strands) and to the cryo-plant burden to remove the operational heat load. The design leading to the minimum cost while still complying with a $\Delta T_{CS}^{min} > 2K$ is then identified.

II. METHODOLOGY

The techno-economic optimization performed here is based on one side on the evaluation of the conductor performance in terms of compliance with the hot spot temperature criterion and minimum temperature margin criteria.

The hot spot temperatures, T_{HS} , have been calculated by solving the adiabatic hot-spot model [13] in (1):

$$\int_{T_{op}}^{T_{HS}} \frac{\bar{c}(T)}{\rho(T)} dT = \int_0^{\infty} dt J_{Cu}^2 \quad (1)$$

where T_{op} is the operating temperature, ρ is the electrical resistivity of the Copper (Cu) (Residual Resistivity Ratio = 150), \bar{c} is the averaged heat capacity per unit volume, and J_{Cu} is the current density after quench. In the calculation, it is assumed, conservatively, that all the current flows in the Cu cross-section A_{Cu} . The temperature- and field-dependent resistivity of Cu is taken from [14] and [15]. The delay time starting from the origin of the quench until the beginning of the current discharge is set to 1.5 s, whereas the characteristic time constant of the circuit following a quench is set to 5 s. The averaged volumetric heat capacity is calculated as in (2), where θ is the angle between the feeder axis and the strand axis and A_{TOT} is the total cross-section:

$$\bar{c} = \frac{c_{p,Cu} A_{Cu} + c_{p,NbTi} A_{NbTi} + c_{p,He} A_{He} + c_{p,SS} A_{SS}}{A_{TOT} \cos(\theta)} \quad (2)$$

The heat capacity data per unit volume (c_p) are taken from [16], [17], and [18] for solids and from [19] for the Helium (He).

The adopted criterion on T_{HS} is such that during a quench it should not exceed 150 K ($T_{HS,1}$), accounting for the heat transfer to the (stagnant) helium. If only the Cu and NbTi are considered ($A_{He} = A_{SS} = 0$), then the maximum allowable adiabatic hot spot temperature is set to 250 K as done in ITER ($T_{HS,2}$).

The temperature margin to current sharing ΔT_{CS}^{min} is defined on the basis of the local current sharing temperature $T_{CS}(x)$ and of the local strand temperature $T_{St}(x)$ as

$$\Delta T_{CS}^{min} = \min_{0 \leq x \leq L} (T_{CS}(x) - T_{St}(x)) \quad (3)$$

In (3), x is the local coordinate along the feeders and L is their length. The thermal-hydraulic analysis for the performance assessment has been performed using the software OPENSC² [20]. A mass flow rate between 0.1 g/s and 10 g/s of Supercritical Helium (SHe) at 0.5 MPa and 4.5 K has been considered as coolant, in all cases entering the conductor from the high-field side. Joule heating is accounted in the 0.47 m-long joints (joint resistance = 5nΩ) located at both inlet and outlet of the feeder. Radiation from the thermal shield at 80 K has been conservatively considered on the 70% of the external surface of all feeders (emissivity $\epsilon = 0.89$), while conduction heating from feeder supports is neglected in view of the lack of information about the mechanical support of the feeders.

On the other, more economical, side, a cost function for the feeders (C_{tot}) is built here, based on features that are related both to their manufacturing (C_{SC+Cu}) and to the operating costs ($C_{cryoplant}$) as in (4).

$$C_{tot} \sim C_{cryoplant} + C_{SC+Cu} \quad (4)$$

The manufacturing costs are related to the manufacture complexity and are split here in costs per unit length for a NbTi strand (C_{NbTi}) and a segregated copper strand ($C_{Cu,segr}$), to be multiplied by the number of SC strands N_{SC} and copper strands $N_{Cu,segr}$, respectively, and the cost of the cabling per unit length $C_{cabl-jack}$:

$$C_{SC+Cu} = L \times (C_{NbTi} \times N_{SC} + C_{Cu,segr} \times N_{Cu,segr} + C_{cabl-jack}) \quad (5)$$

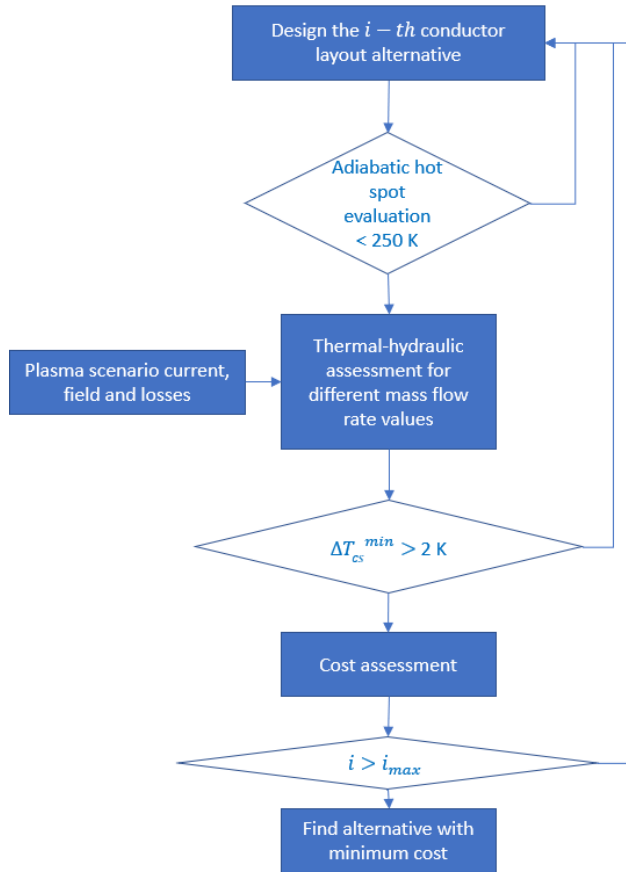


FIGURE 2. Flowchart of the techno-economical optimization performed within this work.

The actual values considered here for the specific costs of the strands are 150 €/kg for the NbTi and 42 €/kg for the segregated copper, whereas the average linear density is 4.2 kg/km and 4.7 kg/km for a NbTi and a Cu strand, respectively. The cabling is rated to 400 k€/km for a conductor with 5 cabling stages.

As far as the cryoplant is considered, $C_{cryoplant}$ is given by the sum of three contributions, and namely the cost of heat removal at cryogenic temperature C_{power} , the maintenance cost C_{maint} and the pumping cost C_{pump} . The last two are considered negligible in this analysis since the contribution due to the feeder to the total maintenance and pumping costs can be considered negligible when compared to that due to the cooling of the rest of the magnets, so that

$$C_{cryoplant} \sim C_{power} + C_{maint} + C_{pump} \sim C_{power} \quad (6)$$

The contribution of C_{power} is proportional to the average power to be removed at cryogenic temperature from the feeders P_{ave} . Note that, if we consider an inverse thermodynamic cycle operating between the ambient temperature T_{amb} and the cryogenic temperature T_{op} , the power removed at cryogenic temperature gives the electrical power P_{feeder} that is needed to provide such cooling if the inverse cycle has an

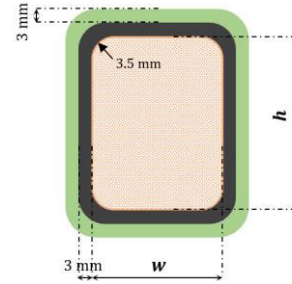


FIGURE 3. Schematic view of the DTT feeder CICC.

efficiency η (here 20% as suggested in [21]):

$$P_{feeder} = \frac{1}{\eta} \frac{T_{amb} - T_{op}}{T_{op}} P_{ave} \sim 320 P_{ave} \quad (7)$$

The annual operating costs of the cryoplant are then given by (8), where θ represents the operating hours/year and e the electricity cost.

$$C_{power} = e \times \theta \times P_{feeder} \quad (8)$$

The methodology followed for the optimization of each feeder is depicted in the flow chart in Fig. 2.

III. ALTERNATIVE FEEDER CONDUCTOR LAYOUTS

The first design of the DTT magnet feeders, together with their routing in around the tokamak, has already been described and discussed in [10]. For the 6 CS modules, 2 feeders per module are present and sized to transport a current of 32 kA at the peak magnetic field of 4 T. For the 6 PF coils, 2 feeders per coil are foreseen and sized again to transport a current of 32 kA but at a lower field (3.1 T). The 18 TF coils are connected in series in groups of 6 coils: they present 3×2 feed-and-return feeders and 3×5 jumpers, connecting two TF coils. The transport current for the TF coils feeders and jumpers is 42.5 kA, with a peak field of 1.4 T. All the feeder conductors are designed as 5-stages twisted cables, assembled using commercial NbTi strands (with 1914 0.011-mm SC filaments) with a diameter of 0.82 mm and, if needed, pure Cu segregated strands as stabilizer. All cables are contained in rectangular SS316L conduits (see Fig. 3) with different dimensions, according to the final number of strands, and void fraction around 35%, resulting in classical 1-region CICC, for which a 3-mm prepreg fiberglass insulation layer is foreseen.

From preliminary analysis of the feeder DC performance [10], the 16.6 m-long CS3U2 feeder, the 7.3 m-long PF61 feeder and the 3.25 m-long TF jumpers turned out to be the most critical ones, i.e. the ones with the minimum temperature margin to current sharing ΔT_{CS}^{min} , defined as the minimum local difference between the current sharing and the cable operating temperatures.

A. CS FEEDER LAYOUTS

Three alternative layouts (B, C, D layouts in Table 1) for the CS feeders were developed and analyzed on top of the baseline layout (layout A in Table 1) already presented in [10].

TABLE 1. Different alternatives for the CS feeder layouts.

Layout	N_{SC}	$N_{Cu,segr}$	h [mm]	w [mm]
A	1350	0	37.88	30.30
B	540	270	29.38	23.50
C	360	720	33.81	27.05
D	324	162	22.88	18.30

TABLE 2. Different alternatives for the feeder layouts of PF and TF coils.

Layout	N_{SC}	$N_{Cu,segr}$	h [mm]	w [mm]
A1	162	324	22.88	18.30
B1	144	288	21.56	17.25
C1	135	270	20.94	16.75

The alternative layouts are developed based again on the scaling from the critical current in [11], but with a progressively reduced number of SC strands N_{SC} and increasingly higher number of segregated Cu strands $N_{Cu,segr}$. While the first and the last of the cabling stages are kept fixed to the classical twisting pitch of 3 triplets of (SC/Cu) wires, and 6 petals, respectively, the intermediate stages are modified from the original 5×5 pattern (layout A) to 3×5 (layout B), 4×5 (layout C) and eventually 3×3 (layout D). As a consequence of the almost constant void fraction of the conductor, the dimensions of the conductor (h and w in Table 2, see Fig. 3) also vary.

B. PF COIL FEEDER LAYOUTS

Two alternative layouts (B1 and C1 in Table 2) were developed and analyzed for the PF coils, in addition to the baseline layout (A1 in Table 2) [10]. Again, the number N_{SC} in decreasing throughout the alternatives, and they also differ for $N_{Cu,segr}$ and for the conductor cross section dimension. For these feeders, the cabling pattern was varied from the original pattern of (1 SC + 2 Cu) $3 \times 3 \times 3 \times 6$ (layout A1) modifying the last two stages in 3×5 (layout B1) and 4×4 (layout C1).

C. TF COIL FEEDER AND JUMPER LAYOUTS

The same alternatives analyzed for the PF coils were retained for the analysis of the TF feeders as well.

IV. HEAT LOADS TO FEEDERS DURING PLASMA OPERATION

We consider here a standard single-null (SN) plasma operating scenario (V12) [2], [22], sketchily shown in Fig. 4.

A. EVALUATION OF THE AC LOSSES

The reference model for the AC losses adopted here is sketched in Fig. 5, where the coupling currents in the wires with twisted filaments are shown.

The overall AC losses are then given by the sum of the contribution of the coupling losses M_c , of the hysteresis losses



FIGURE 4. Timeline of the standard SN plasma operating scenario considered in the present analysis.

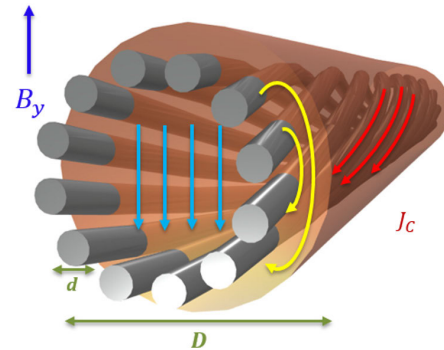


FIGURE 5. Sketch of the coupling currents within the SC strand when the external field is varied in the vertical direction.

M_h and of the dynamic resistance losses V_d as [23]:

$$P_{AC,tot} = \frac{1}{\mu_0} (M_c + M_h) \dot{B} + \frac{V_d I_t}{A} \quad (9)$$

The three contributions are detailed in (10)-(12).

$$M_c = \begin{cases} \tau |\dot{B}| - \frac{1}{2} \frac{(\tau \dot{B})^2}{B_p} & \tau |\dot{B}| \leq B_p^* \\ \frac{1}{2} B_p (1 - i^2) & \tau |\dot{B}| > B_p^* \end{cases} \quad (10)$$

$$M_h = \begin{cases} \frac{b_p}{2} \left(1 - \frac{\tau |\dot{B}|}{B_p} \right) \left(1 - \frac{i^2}{\left(1 - \frac{\tau |\dot{B}|}{B_p} \right)^2} \right) & \tau |\dot{B}| \leq B_p^* \\ 0 & \tau |\dot{B}| > B_p^* \end{cases} \quad (11)$$

$$V_d = \begin{cases} \frac{1}{2} di |\dot{B}| \left(1 - \frac{\tau |\dot{B}|}{B_p} \right)^{-1} & \tau |\dot{B}| \leq B_p^* \\ \frac{1}{2} di |\dot{B}_e| + \frac{1}{2} Di |\dot{B}_e| \left(1 - \frac{B_p^*}{\tau |\dot{B}_e|} \right) & \tau |\dot{B}| > B_p^* \end{cases} \quad (12)$$

being d the filament diameter, the reduced current i defined as the ratio of the transport current I_t to the critical current I_c and B_p^* defined by (13) as a function of the full-penetration field of the composite conductor B_p [23] in (14):

$$B_p^* = B_p (1 - i) \quad (13)$$

$$B_p = 2\mu_0 \frac{I_c}{\pi D} \quad (14)$$

In (12)-(14), D is the composite diameter.

In (11), the penetration field of the filament b_p , is defined as:

$$b_p = 2\mu_0 \frac{I_c}{\pi d} \quad (15)$$

being d the filament diameter.

The magnetic field B is obtained solving numerically the Ogasawara equation [23], [24]:

$$B_e - B = \frac{\tau \dot{B}}{1 + \frac{\tau \dot{B}}{B_p}} \quad (16)$$

in which B_e represents the changing external field, whereas the decay time constant of the induced coupling currents τ , is defined as:

$$\tau = \frac{\mu_0}{\rho_{et}} \left(\frac{l_p}{2\pi} \right)^2 \quad (17)$$

where l_p is the twist pitch, and ρ_{et} the effective resistivity of the Copper stabilizing matrix.

Note that the coupling time constant is a crucial parameter in the calculation of the coupling loss. In a CICC, the coupling currents loss account for the multiple induced currents loops with a broad range of time constant, affecting different volume fractions of the cable [25]. By using a single time constant, we implicitly assume that only one contribution is dominant at all time. This parameter is affected by a certain degree of uncertainty, due to the experimental difficulty of determining its value accurately. In principle, τ is expected to be different in the two types of feeders, since it depends on the composite and cable layouts. However, in the simulations the same value (150 ms) has been used, based on the values previously measured on other CICC's with similar layouts.

B. EVALUATION OF THE NUCLEAR HEAT LOAD

The nuclear heat load has been considered only for the TF feeders, and conservatively taken as 0.1 mW/cm^3 , in agreement to the values on the outermost part of the TF casing, as shown in [26].

V. RESULTS

The computed results on the alternative cable configurations for the different feeders is first performed in terms of T_{HS} and then in terms of ΔT_{CS}^{min} in operation. Eventually, the economic performance is assessed to identify the best options.

A. EVALUATION OF $T_{HOTSPOT}$

The computed values of the hot-spot temperatures, computed accounting for, or neglecting, the heat sink constituted by the helium, are reported in Table 3, showing that for all the adopted layouts the constraint of 150K for the “wetted” conductor is always satisfied, while the constraint on the “dry” conductor ($T_{HS,2} < 250 \text{ K}$) is largely not met for the second layout (B1) of the TF jumper, and just slightly overcome when the layout C1 is considered. All the alternative layouts for the CS and PF coils feeders show hot spot temperature values well below the design criteria.

B. HEAT LOSSES

From the computed magnetic field and magnetic field variation, according also to the transport current shown in Fig. 6a, the computed AC losses per unit length and single SC strand

TABLE 3. Hot-spot temperature for the different cable configurations.

Feeder	Layout	$T_{HS,1}$ (K)	$T_{HS,2}$ (K)
CS	A	23	37
	B	34	50
	C	57	105
	D	22	38
PF	A1	43	79
	B1	54	124
	C1	49	103
TF jumper	A1	62	158
	B1	85	381
	C1	75	266

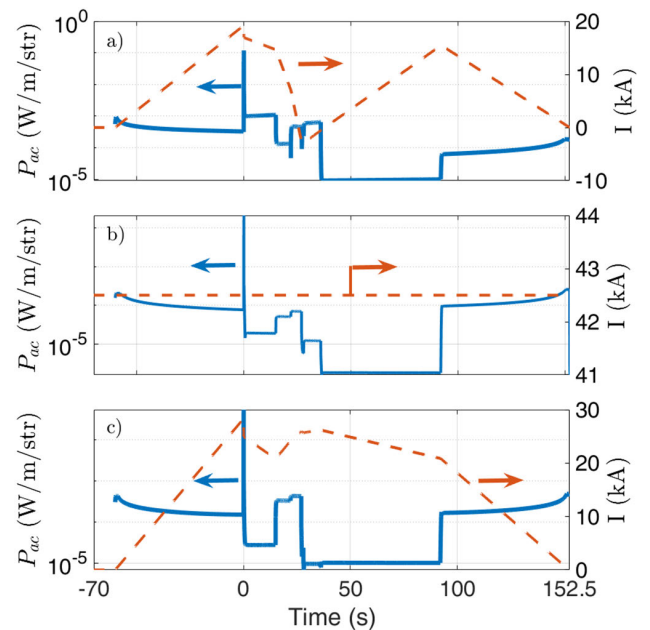


FIGURE 6. Computed AC loss per unit length and per strand (blue lines, left axes) and transport current (red lines, right axes) in the CS3U2 feeder (a), in the PF61 coil feeder (b) and in the TF jumper (c), respectively.

turned out to be constant for all the configurations of each feeder, and they are shown in Fig. 6b. Note that the scale of the y axis is logarithmic, and the deposited power can reach almost 1 W/m at the plasma breakdown in the CS feeder.

The resulting power, averaged on the entire plasma pulse, is shown in Figs. 7-8. More in detail, in Fig. 7a the average power for the different configurations of the CS3U2 feeder is shown. The dominant contribution for the CS feeder is given by the AC losses, which can vary up to a factor of 3 for the different configurations, in view of the very large difference in N_{SC} they present, see Table 1. The impact of the AC losses is significantly reduced when one considers the different configurations of the PF61 feeder (see Fig. 7b noting the different scale if compared to Fig. 7a), where the global losses are dominated by Joule power. The AC

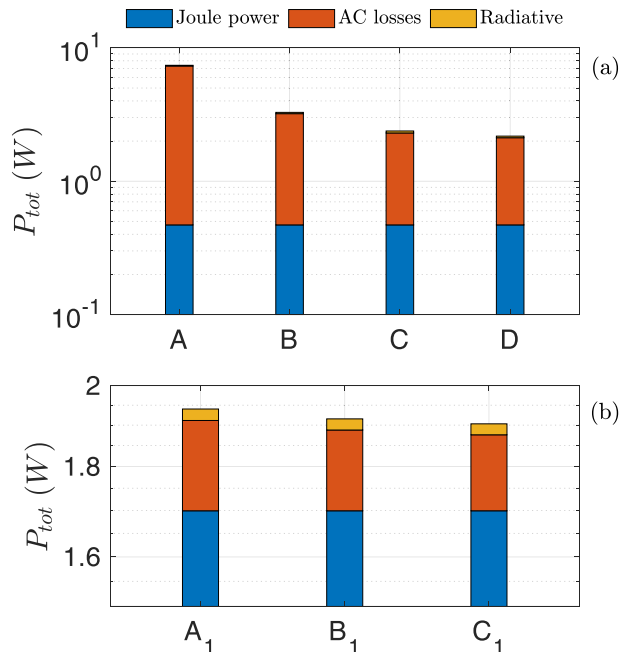


FIGURE 7. Average power, split by components (Joule from the joints, AC and radiative), on the different configurations of the CS3U2 feeder (a) and on the PF61 feeder (b), respectively, during the plasma pulse under investigation and for a He mass flow rate of 5 g/s.

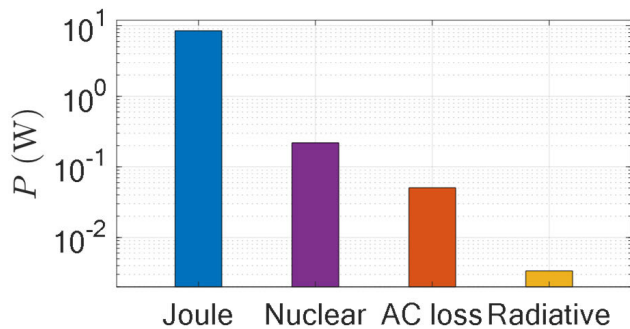


FIGURE 8. Average power, split by components (Joule from the joints, nuclear, AC and radiative), on configuration A1 of the TF jumper, during the plasma pulse under investigation and for a He mass flow rate of 5 g/s.

loss contribution becomes almost totally negligible, if the TF feeder is investigated (see Fig. 8, where the scale in the y axis is logarithmic). For the TF feeder, indeed, the static load is by far the dominant component, as expected.

C. PERFORMANCE ASSESSMENT

The computed minimum temperature margin along each feeder, considering different configurations and different possible values for the nominal mass flow rate are reported in Fig. 9.

As far as the CS3U2 feeder is concerned, the value of ΔT_{CS}^{min} is always computed when the losses are highest (breakdown) independently on configuration and flow rate (provided it is > 0.5 g/s). Being the losses per cycle proportional to N_{SC} , the temperature margin turns out to be quite insensitive to it, as visible in Fig. 9a, where the margin varies by 15% throughout the entire parameter space explored in

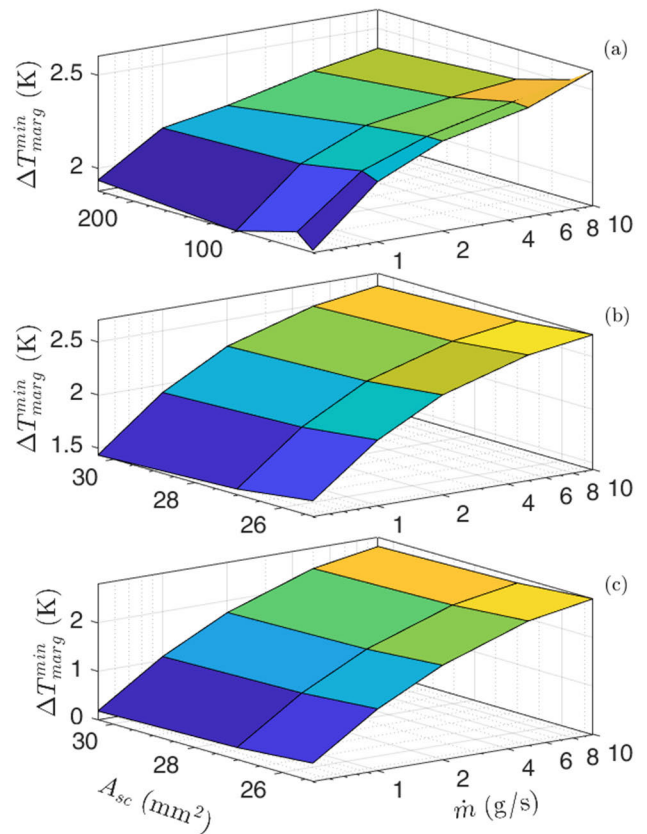


FIGURE 9. Minimum temperature margin computed for the different configurations for different values of the mass flow rate for the CS3U2 feeder (a), PF61 feeder (b) and TF jumper (c), respectively.

the analysis and it is basically unaffected by the value of the coolant flow rate.

The behaviour of the PF61 feeder and TF jumper is different in that respect (see Figs. 9b,c), since there is a larger effect of the coolant flow rate in the temperature margin. Note, however, that in these two cases the amount of SC material in the cable has been varied in a much smaller range, if compared to the configurations analysed for the CS3U2 feeder. For the TF jumper, moreover, only for mass flow rates ≥ 5 g/s guarantee the margin > 2 K for all configurations (Fig. 9c).

The hydraulic performance of the different conductor layouts is reported in Fig. 10 for the sake of completeness. For all the layouts of the TF/PF coils feeder, as well as for the layout D of the CS feeders, the pressure gradient reaches about 1 kPa/m if the Katheder correlation is used [27]. Note that the computed values is, at a mass flow rate of 10 g/s, 1 order of magnitude larger than the reference values typically computed for the (ITER-like) two-regions CICC, where a low-impedance relief central channel is present [28], [29]. The much larger pressure gradient is largely compensated by the short lengths into play (max 17.6 m for the CS feeders and < 12 m for all the others).

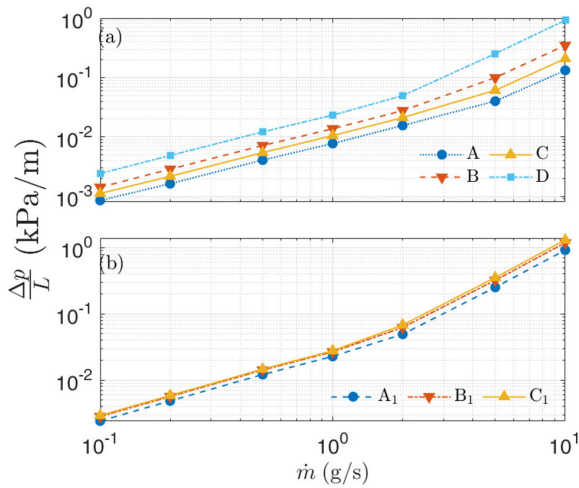


FIGURE 10. Hydraulic characteristic of the different feeder layouts for the CS (a) and the TF and PF coils (b).

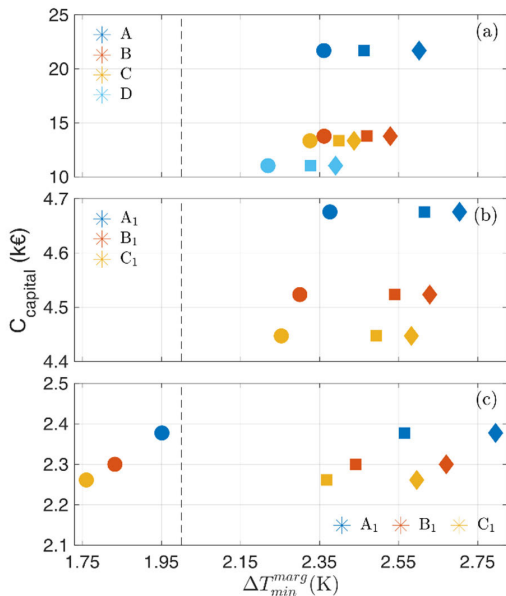


FIGURE 11. Capital cost estimated for the CS3U2 feeder (a), PF61 feeder (b) and TF jumper (c), respectively, reported as a function of the computed minimum temperature margin during the investigated plasma pulse, for different configurations and operating mass flow rate values: circle 2 g/s, square 5 g/s, diamond 10 g/s, respectively. The value of ΔT_{CS}^{min} is also reported (dashed line).

D. ECONOMIC ASSESSMENT

The capital cost of the different cable layouts from (3) gives the results reported in Fig. 11. It is clear that the alternative configurations for CS feeder conductors can allow saving up to 50% of the capital cost (Fig. 11a), while still keeping the temperature margin above 2 K, at all the considered mass flow rates > 2 g/s. The saving for the PF feeders could achieve only ~ 10%, but with some additional room for improvement (Fig. 11b), especially if the nominal mass flow rate is targeted, for which the temperature margin is 2.5 K. No effect on the conductor cost of the alternative configurations for the TF jumpers is found (Fig. 11c), also keeping in mind the poor

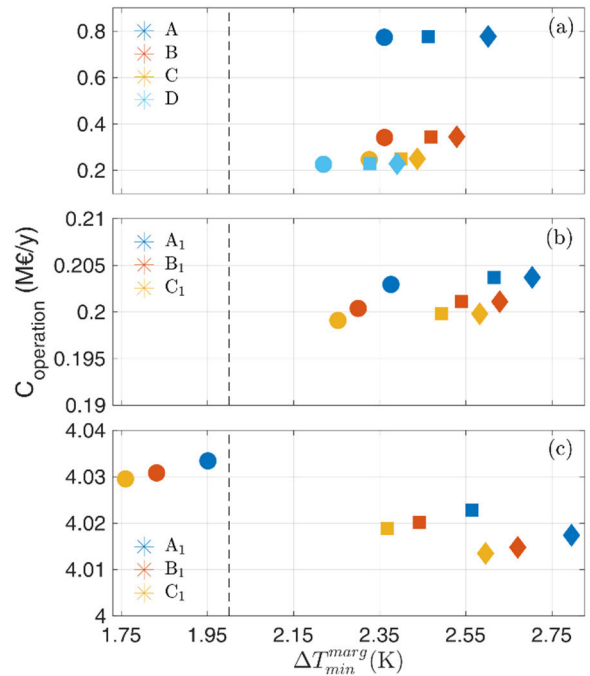


FIGURE 12. Operation cost per year estimated for the CS3U2 feeder (a), PF61 feeder (b) and TF jumper (c), respectively, reported as a function of the computed minimum temperature margin during the investigated plasma pulse, for different configurations and operating mass flow rate values: circle 2 g/s, square 5 g/s, diamond 10 g/s, respectively. The value of ΔT_{CS}^{min} is also reported (dashed line).

performance in terms of $T_{HS,2}$ of the two alternative layouts. Note that the different capital cost for the TF coil jumper, compared to the PF coil feeder, derives from the different lengths of the two conductors, while the cost per unit length is obviously the same, and very similar to that of the layout D of the CS feeders.

Moving to the operational costs of the cryoplant, we consider one year of operation, with a constant electricity cost of 0.3 €/kWh. For the CS3U2 and PF61 coil feeders an operation time of 1000 h/y is considered, while for the TF jumper an operation time of 180 d/y is accounted for. The results in terms of cost of operation of a single feeder are reported in Fig. 12, where the cost related to the pumping power of the coolant has been neglected since the total mass flow rate for the feeders is small compared to that of the magnet system. The cost associated to the CS3U2 feeder are strongly influenced by the alternatives (Fig. 12a) since the AC loss power is strongly related to N_{SC} , which varies by a factor of 4 among the different alternatives. For the same reason, the cost of the other feeders is almost unaffected changing the configuration (Fig. 12b, c). Note that the operational cost of the TF jumper is one order of magnitude higher than that of the feeders of the pulsed coils, in view of the much longer operational time foreseen for the TF coils. This aspect becomes even more critical keeping in mind that the largest fraction of the power to be removed from the TF jumper is the Joule load on the joints, and that the TF jumpers and feeders

are much more than the feeders of the pulsed coils (namely 15 jumpers and 3×2 feeders).

VI. CONCLUSION

A techno-economic assessment on different cable alternatives for the DTT feeders has been performed, evaluating different key performance indicators, and namely the capability to meet the criteria on the maximum hot spot temperature, the capability to meet the criterion on the minimum temperature margin during operation, the hydraulic performance and the capital and operational costs.

The results highlight that there is room for $\sim 50\%$ saving in the capital cost for the pulsed CS feeders found, moving from the original layout (A) to layout D, reducing to 25% of the number of SC strands and introducing segregated-copper strands. Also, the operational cost could be dramatically reduced if layout D is implemented for the CS feeders instead of the original one.

As far as the PF coil feeders are concerned, a saving of 5% in the capital cost can be achieved by moving from the original layout (A1) to a cable again with a reduced number of SC strands (layout C1).

Notwithstanding a comparable capital cost per unit length of the cable, the TF coil feeders are anticipated to have a $20\times$ operational cost, when compared to the others. The original design for the TF coil feeders has been confirmed here to be the best among the alternative configurations considered, guaranteeing the highest minimum temperature margin without significant increase of the operational costs.

REFERENCES

- [1] T. Donné, "European research roadmap to the realisation of fusion energy," EUROfusion, Garching, Germany, 2018.
- [2] R. Ambrosino, "DTT—Divertor tokamak test facility: A testbed for DEMO," *Fusion Eng. Des.*, vol. 167, Jun. 2021, Art. no. 112330, doi: [10.1016/J.FUSENGDES.2021.112330](https://doi.org/10.1016/J.FUSENGDES.2021.112330).
- [3] A. D. Zenobio et al., "DTT: A challenging framework for a sound superconducting magnets design," *IEEE Trans. Appl. Supercond.*, vol. 32, no. 6, pp. 1–5, Sep. 2022, doi: [10.1109/TASC.2022.3153235](https://doi.org/10.1109/TASC.2022.3153235).
- [4] G. S. Lee et al., "The design of the KSTAR tokamak," *Fusion Eng. Des.*, vol. 46, nos. 2–4, pp. 405–411, Nov. 1999, doi: [10.1016/S0920-3796\(99\)00032-0](https://doi.org/10.1016/S0920-3796(99)00032-0).
- [5] P. D. Weng, "The engineering design of the HT-7U tokamak," *Fusion Eng. Des.*, vols. 58–59, pp. 827–831, Nov. 2001, doi: [10.1016/S0920-3796\(01\)00479-3](https://doi.org/10.1016/S0920-3796(01)00479-3).
- [6] E. Di Pietro, P. Barabaschi, Y. Kamada, and S. Ishida, "Overview of engineering design, manufacturing and assembly of JT-60SA machine," *Fusion Eng. Des.*, vol. 89, pp. 2128–2135, Oct. 2014, doi: [10.1016/J.FUSENGDES.2013.11.015](https://doi.org/10.1016/J.FUSENGDES.2013.11.015).
- [7] *ITER—The Way to New Energy*. Accessed: Oct. 30, 2022. [Online]. Available: <https://www.iter.org/>
- [8] A. J. Creely et al., "Overview of the SPARC tokamak," *J. Plasma Phys.*, vol. 86, no. 5, Oct. 2020, Art. no. 865860502, doi: [10.1017/S0022377820001257](https://doi.org/10.1017/S0022377820001257).
- [9] L. Muzzi, G. De Marzi, A. Di Zenobio, and A. D. Corte, "Cable-in-conduit conductors: Lessons from the recent past for future developments with low and high temperature superconductors," *Supercond. Sci. Technol.*, vol. 28, no. 5, Mar. 2015, Art. no. 053001, doi: [10.1088/0953-2048/28/5/053001](https://doi.org/10.1088/0953-2048/28/5/053001).
- [10] D. Placido, G. De Marzi, A. Di Zenobio, G. Ramogida, L. Savoldi, and S. Viarengo, "Evaluation of the thermal performance of the SC feeders for the magnetic system of the divertor tokamak test facility," *IEEE Trans. Appl. Supercond.*, vol. 32, no. 6, Sep. 2022, Art. no. 4202605, doi: [10.1109/TASC.2022.3161249](https://doi.org/10.1109/TASC.2022.3161249).
- [11] L. Muzzi, G. De Marzi, C. F. Zignani, L. Affinito, M. Napolitano, R. Viola, C. O. Dominguez, L. Bottura, S. Le Naour, D. Richter, and A. D. Corte, "Pinning properties of commercial Nb-Ti wires described by a 2-components model," *IEEE Trans. Appl. Supercond.*, vol. 20, no. 3, pp. 1496–1499, Jun. 2010, doi: [10.1109/TASC.2009.2039124](https://doi.org/10.1109/TASC.2009.2039124).
- [12] R. Villari, M. Angelone, B. Caiffi, A. Colangeli, F. Crisanti, D. Flammini, N. Fomesu, R. Luis, G. Mariano, D. Marocco, F. Moro, G. M. Polli, and S. Sandri, "Nuclear design of divertor tokamak test (DTT) facility," *Fusion Eng. Des.*, vol. 155, Jun. 2020, Art. no. 111551, doi: [10.1016/J.FUSENGDES.2020.111551](https://doi.org/10.1016/J.FUSENGDES.2020.111551).
- [13] M. Calvi, P. Bauer, D. Bessette, F. Cau, C. Marinucci, and P. Bruzzone, "Design proposal for the ITER feeder busbars," *IEEE Trans. Appl. Supercond.*, vol. 20, no. 3, pp. 407–410, Jun. 2010, doi: [10.1109/TASC.2010.2041535](https://doi.org/10.1109/TASC.2010.2041535).
- [14] P. Bauer, H. Rajainmaki, and E. Salpietro, "EFDA material data compilation for superconductor simulation," Eur. Fusion Develop. Agreement-Close Support Unit, Garching, Tech. Rep., 2007.
- [15] N. J. Simon, E. S. Drexler, and R. P. Reed, "Properties of copper and copper alloys at cryogenic temperatures," U.S. Dept. Energy Office Sci. Tech. Inf., USA, Final Rep. PB-92-172766/XAB; NIST/MONO-177, Feb. 1992, doi: [10.2172/5340308](https://doi.org/10.2172/5340308).
- [16] L. Dresner, *Stability of Superconductors*. Norwell, MA, USA: Kluwer, 2002.
- [17] S. A. Elrod, J. R. Miller and L. Dresner, "The specific heat of NbTi from 0 to 7 T between 4.2 and 20 K," in *Advances in Cryogenic Engineering Materials*, vol. 28, R. P. Reed, and A. F. Clark, Eds. Boston, MA, USA: Springer, 1982, doi: [10.1007/978-1-4613-3542-9_60](https://doi.org/10.1007/978-1-4613-3542-9_60).
- [18] *Thermal, Electrical and Mechanical Properties of Materials at Cryogenic Temperatures, Superconducting Material Database, Article 5, No. 11, FDR 42, Release 0.1*, ITER DRG1 Annex, Saint-Paul-lez-Durance, France, Jul. 5.
- [19] *HEPAK*. Accessed: Dec. 5, 2022. [Online]. Available: <https://htess.com/hepak/>
- [20] L. Savoldi, D. Placido, and S. Viarengo, "Thermal-hydraulic analysis of superconducting cables for energy applications with a novel open object-oriented software: OPENSC2," *Cryogenics*, vol. 124, Jun. 2022, Art. no. 103457.
- [21] R. Guarino, R. Wesche, and K. Sedlak, "Technical and economic feasibility study of high-current HTS bus bars for fusion reactors," *Phys. C, Supercond. Appl.*, vol. 592, Jan. 2022, Art. no. 1353996, doi: [10.1016/J.PHYSC.2021.1353996](https://doi.org/10.1016/J.PHYSC.2021.1353996).
- [22] A. Castaldo, R. Albanese, R. Ambrosino, and F. Crisanti, "Plasma scenarios for the DTT tokamak with optimized poloidal field coil current waveforms," *Energies*, vol. 15, no. 5, p. 1702, Feb. 2022, doi: [10.3390/EN15051702](https://doi.org/10.3390/EN15051702).
- [23] T. Ogasawara, Y. Takahashi, K. Kanbara, Y. Kubota, K. Yasohama, and K. Yasukochi, "Transient field losses in multifilamentary composite conductors carrying DC transport currents," *Cryogenics*, vol. 20, no. 4, pp. 216–222, Apr. 1980, doi: [10.1016/0011-2275\(80\)90130-7](https://doi.org/10.1016/0011-2275(80)90130-7).
- [24] G. De Marzi, L. Muzzi, M. Breschi, L. Cavallucci, D. Uglietti, and A. D. Corte, "Numerical studies of high field-rate losses in cable-in-conduit-conductors carrying transport current," in *Proc. CHATS Appl. Supercond.*, 2021, p. 1.
- [25] P. Bruzzone, B. Stepanov, K. Sedlak, and V. Corato, "A new test method of AC loss assessment for fusion conductors," *Fusion Eng. Des.*, vol. 146, pp. 928–931, Sep. 2019, doi: [10.1016/J.FUSENGDES.2019.01.116](https://doi.org/10.1016/J.FUSENGDES.2019.01.116).
- [26] R. Bonifetto, A. D. Zenobio, L. Muzzi, S. Turtu, R. Zanino, and A. Zappatore, "Thermal-hydraulic analysis of the DTT toroidal field magnets in DC operation," *IEEE Trans. Appl. Supercond.*, vol. 30, no. 4, pp. 1–5, Jun. 2020, doi: [10.1109/TASC.2020.2964517](https://doi.org/10.1109/TASC.2020.2964517).
- [27] H. Katheder, "Optimum thermohydraulic operation regime for cable in conduit superconductors (CICS)," *Cryogenics*, vol. 34, pp. 595–598, Jan. 1994, doi: [10.1016/S0011-2275\(05\)80139-0](https://doi.org/10.1016/S0011-2275(05)80139-0).
- [28] R. Zanino and L. S. Richard, "A review of thermal-hydraulic issues in ITER cable-in-conduit conductors," *Cryogenics*, vol. 46, nos. 7–8, pp. 541–555, Jul. 2006, doi: [10.1016/J.CRYOGENICS.2006.01.007](https://doi.org/10.1016/J.CRYOGENICS.2006.01.007).
- [29] C. Marinucci, P. Bruzzone, A. D. Corte, L. S. Richard, and R. Zanino, "Pressure drop of the ITER PFCI cable-in-conduit conductor," *IEEE Trans. Appl. Supercond.*, vol. 15, no. 2, pp. 1383–1386, Jun. 2005, doi: [10.1109/TASC.2005.849096](https://doi.org/10.1109/TASC.2005.849096).



DANIELE PLACIDO was born in Melfi in 1995. He received the M.Sc. degree in energy and nuclear engineering from the Politecnico di Torino, Torino, Italy, in 2020, where he is currently pursuing the Ph.D. degree in energetics at Dipartimento Energia “Galileo Ferraris.”

The research he is carrying on concerns the development of an open-access software for the analysis of electro-magnetic and thermal-hydraulic transients in superconducting cables for fusion and power applications, cooled by a cryogen in forced flow.

Mr. Placido is a member of the MAHTEP Group, Politecnico di Torino. In 2022, he received an Award for the Best M.Sc. Thesis in the field of thermal-fluid dynamics with his Thesis: “Object-oriented modeling of LTS and HTS superconducting cables” from the Thermal-fluid dynamics Italian Union.



GIANLUCA DE MARZI received the M.Sc. degree (cum laude) in physics and the Ph.D. degree in material sciences from the University of Rome La Sapienza, Italy, in 1996 and 2000, respectively. He is currently a Staff Researcher with the Superconductivity Laboratory, Italian National Agency for New Technologies, Energy and Sustainable Economic Development (ENEA) at Frascati, Rome. His current research activities are focused on the design and manufacturing of superconducting cables, conductors, and magnets, for nuclear fusion experiments.

Dr. De Marzi is currently a Task Responsible for the design of the superconducting magnet system’s current feeders for the Divertor Tokamak Test (DTT) facility. He is a Technical Editor of the IEEE TRANSACTIONS ON APPLIED SUPERCONDUCTIVITY.



LUIGI MUZZI (Senior Member, IEEE) received the Degree in physics from the University of Rome La Sapienza, Italy, in 1999, and the Ph.D. degree in condensed matter physics from the University of Rome Tor Vergata in 2003. He is a Researcher at the Superconductivity Section of the Italian research Agency ENEA, he has worked on the study and characterization of superconducting materials, cables and magnets for fusion application, participating to the main projects in the field,

among which JT-60SA, ITER and the EU-DEMO. He is the Project Leader for the Central Solenoid of the Italian tokamak DTT and also a Production Manager of the ICAS Company, he coordinates the manufacturing activities of superconducting cables at the industrial partner, TRATOS Cavi. He has authored or coauthored over 150 articles in international scientific journals;

Dr. Muzzi is a Technical Editor for the IEEE TRANSACTIONS ON APPLIED SUPERCONDUCTIVITY and he has been serving as a Program Committee Member for the Applied Superconductivity and for the Magnet Technology Conferences since 2014.



LAURA SAVOLDI (Member, IEEE) received the M.Sc. degree (cum laude) in nuclear engineering and the Ph.D. degree in energetics from the Politecnico di Torino, Torino, Italy. She is currently serves as a Full Professor in nuclear plants at the Politecnico di Torino. In this frame, she developed the 4C code for the analysis of thermal-hydraulic transients in superconducting cables, coils and related cryogenic circuits. She co-authored 200+ papers published in international

journals and proceedings of international conferences. Her research interests are in the development, validation, and application of computational tools for the analysis of thermal-hydraulic transients in advanced heat transfer problems, including super-conducting magnets.

Prof. Savoldi serves as a referee for several international journals and conferences of her field of research, among which IEEE TRANSACTIONS ON APPLIED SUPERCONDUCTIVITY and IEEE TRANSACTIONS ON PLASMA SCIENCE.

• • •

Open Access funding provided by ‘Politecnico di Torino’ within the CRUI CARE Agreement